FIT-FOR-PURPOSE TREATMENT WITH IRON AND POLYMERIC COAGULANT FOR PRODUCED WATER REUSE IN HYDRAULIC FRACTURING: TEMPERATURE EFFECTS ON AGGREGATION AND SEDIMENTATION

A Thesis

by

MAHITH NADELLA

Submitted to the Office of Graduate and Professional Studies of
Texas A&M University
in partial fulfillment of the requirements for the degree of

MASTER OF SCIENCE

Chair of Committee,	Shankararaman Chellam
Committee Members,	Yossef Elabd
	Mustafa Akbulut
Head of Department,	Robin Autenrieth

August 2019

Major Subject: Civil Engineering

ABSTRACT

Oil and gas well stimulation by hydraulic fracturing necessitates large volumes of water, in turn generating copious amounts of produced water, which is most commonly disposed via deep-well injection. Purifying produced water to a level where it can be reused for additional fracturing addresses the dual challenges of fresh water sourcing and its environmentally conscious disposal. In this manuscript, we systematically investigated fit-for-purpose treatment of produced water for fracking, using the Permian Basin as a test case. Highly saline (~200,000 mg/L total dissolved solids) and turbid (~ 80 NTU) produced water from the Delaware Basin was treated with a combination of $FeCl_3$ as the primary coagulant aided by an anionic polymer to remove suspended solids and iron over a range of environmentally-relevant temperatures via isothermal jar testing. Robust, user-friendly techniques based on mobile phone video capture, optical microscopy, and digital image analysis were developed to accurately characterize floc morphology, size, and settling velocity to interpret experimental data on suspended solids removal. Conformational changes of the polymer over the 4 – 44 °C temperature range were inferred from viscosity and hydrodynamic size measurements providing clues to its performance characteristics. Settling velocities of flocs conformed to a model incorporating their fractal nature, average size, and the viscosity of the suspending medium (i.e. produced water). Juxtaposing the anionic polymer with the hydrolyzing metal-ion coagulant effectively destabilized the suspension through sweep coagulation and adsorption and inter-particle bridging removing ≥ 98% turbidity and ≥ 97% iron allowing reuse of the

produced water for hydraulic fracturing. Although bench-scale laboratory experiments established the efficacy of coagulation-flocculation-sedimentation for suspended solids and iron removal over a wide range of temperatures, we recommend additional larger-scale testing to evaluate process performance under actual field conditions before possible widespread implementation.

ACKNOWLEDGEMENTS

I would like to express my sincere gratitude to my thesis advisor Dr. Shankararaman Chellam for providing me this opportunity of doing world-class research. I am thankful to him for his continuous support, motivation, guidance and immense knowledge. His teaching style and enthusiasm aroused in me the interest to undertake research. I couldn't have imagined a better advisor than him. He was instrumental in not just shaping my thesis but also my personality as a whole.

Besides Dr. Chellam, I would like to thank the rest of my thesis committee: Dr. Yossef Elabd, and Dr. Mustafa Akbulut for their insightful comments and questions which encouraged me to further widen my research from different perspectives.

I am also grateful to my fellow lab mates and friends for continuous motivation and stimulating discussions.

I take this opportunity to express my gratitude to everyone who has contributed directly or indirectly towards this research.

This would not have been possible without the support from my family and friends. This thesis is a testimony to their love and encouragement.

CONTRIBUTORS AND FUNDING SOURCES

Contributors

This work was supervised by a thesis committee headed by Dr. Shankararaman Chellam along with the committee members Dr. Yossef Elabd and Dr. Mustafa Akbulut.

Dynamic light scattering analysis for this project was done in Dr. Mustafa Akbulut's research lab with the help of his PhD student Michael Bae. The highly magnified SEM images of the coagulant flocs were obtained from the Microscopy Imaging Center at Texas A & M University with the help of Dr. Stanlislav Vitha.

All other work conducted for the thesis was completed by the student independently.

Funding sources

There are no outside funding contributions to acknowledge related to the research and compilation of this document.

NOMENCLATURE

ATR-FTIR	Attenuated Total Reflectance-Fourier Transform Infrared
TDS	Total Dissolved Solids
TSS	Total Suspended Solids
DOC	Dissolved Organic Carbon
COD	Chemical Oxygen Demand
TPTZ	2,4,6-Tripyridyl-s-Triazine
PTV	Particle Tracking Velocimetry
$D_{f,2d}$	2D Fractal Dimension
SEM	Scanning Electron Microscopy

TABLE OF CONTENTS

Page

LIST OF FIGURES

Page

LIST OF TABLES

Page

1. INTRODUCTION

The United States is experiencing a renaissance in domestic energy production in part due to oil and natural gas production from unconventional reservoirs. Since 2005, these plays have delivered more than 5 million barrels of oil and 25 billion cubic feet of natural gas. Such dramatic growth has been enabled by (1) the recognition that large volume of hydrocarbons are stored in thermally mature, ultra-low-permeability, organic rich shale rocks and (2) technological advancements that combined and enhanced the efficiency of horizontal drilling and hydraulic fracturing, which led to the invention of high-volume hydraulic fracturing that allowed oil and gas extraction from these plays at commercial rates.

Today, there are more than a dozen unconventional reservoir plays in the United States. Among these, the Permian Basin is considered most prolific given that there are up to 9-10 stacked reservoirs within a vertical depth of ~3000 m [1]. High-volume hydraulic fracturing is centered on the use of large quantities of water to transport proppant (sand) and associated completion fluid additives into the reservoir to create and hold open permeable fractures to allow hydrocarbon extraction. The median values of cumulative water use for horizontal well completion, design lateral well length, (i.e. the length of the horizontally drilled well), and the water use intensity (water use normalized to lateral length of each well) all have increased from 2,460 m^3 to 42,560 m^3, 1,041 to 2013 m, and 2.4 m^3/m to 21.1 m^3/m, respectively from 2008 to 2016 [1, 2]. This represents a 17-fold increase in water use and an 8-fold increase in water intensity. Further, well completion designs are continually evolving with the

potential to further increase water use and intensity [2]. Considering that there are more than 1,900 wells completed annually in the Permian Basin [2], sourcing water for full-field development over a 20 to 25 year period represents a significant problem since it is in short supply in (semi)arid regions of west Texas and southeastern New Mexico.

After a well is completed and put in production, the initial load of water returned back to the surface is referred as "flowback water," which is composed of a blend of injected- and formation water. Over time, the contribution of formation water increases, typically increasing the salinity and is referred as "produced water." Overall, the flowback water volume is small percentage of total water volume that is produced during the life of the well. A larger volume of produced water is generated in the Permian Basin compared to other shale plays [2], with median ratios of water to oil production ranging from ~ 3 to 5 [3]. One report [1], suggests that produced water volumes could be 200-400% in excess of the annual completion source water demand in the Permian Basin, which presents significant operational challenges to its proper management and disposal. Currently, the majority of flowback/produced water is disposed via deep saltwater injection wells [4]. However, this practice induces seismicity especially when injection wells are located near fault lines [5], placing it under increased scrutiny.

Recycling produced water addresses the dual challenges of fresh water sourcing and produced/flowback water disposal [6, 7]. Therefore, many operators in the Permian Basin have begun to investigate and implement large-scale produced

water reuse [8]. Produced water in the Permian is highly turbid with suspended solids concentration reaching as high as 10,000 mg/L [3], which needs to be removed before possible reuse during hydraulic fracturing to minimize the potential for formation damage [6, 9]. It is also highly saline with total dissolved solids concentration > 10%, although salt tolerant fracturing fluids have been recently developed that work well in the presence of monovalent and some divalent cations. A related issue is that of iron, which exists in dissolved form, i.e. Fe(II) under subsurface redox conditions, but oxidizes to insoluble Fe(III) when brought aboveground in the produced water. Particulate iron is incompatible with polymers and other fracturing fluid additives, shields microorganisms from biocides, and presents problems similar to other suspended solids. Hence, iron also needs to be removed to facilitate produced water reuse.

Operators in the Permian Basin are already reusing produced water after removing free oil and solids (including oxidized iron), and inactivating microorganisms [6]. Given the geographic spread of well locations, operators prefer decentralized campaign-style treatment of flowback/produced water using mobile treatment platforms for immediate use in subsequent fracturing programs. Moreover, high-volume hydraulic fracturing requires treated water to be pumped at high rates (80-100 BBL per minute) necessitating a compact treatment footprint while maintaining high suspended solids removal efficiencies. Therefore, many service providers are deploying high-rate clarifiers even though chemical addition for

coagulation and gravity separations for clarification are almost always suboptimal [10].

Hydrolyzing metal ions such as aluminum and iron can be used as coagulants for on-site treatment of produced water [11-13], whose efficacy can be enhanced by adding polymers [14, 15]. The current literature mainly focuses on simple optimization of inorganic metal ion coagulant treatment by adjusting pH, chemical dosage and type, shear rate, residence time, etc. [16-18], lacking detailed analysis of floc characteristics. Further, to our knowledge, incorporating polymers for produced water colloid destabilization in conjunction with sweep coagulation by inorganic coagulants has not yet been rigorously and systematically evaluated. Such a combination has the potential to dramatically improve suspended solids removal [19] potentially resulting in a significantly smaller footprint thereby enhancing portability and throughput; critical field-scale considerations. However, challenges include the higher density and viscosity of produced water especially during cold weather operation [20, 21], which can significantly impede sedimentation.

The primary objectives of this produced water treatment research are to:

- Evaluate synergistic effects of hydrolyzing iron coagulant and polymer addition on colloid destabilization and removal (including particulate iron),
- Develop simple and robust techniques using video and image analysis to characterize floc morphology, size, and settling velocity, and

- Empirically determine process performance and floc characteristics over a range of environmentally relevant temperatures.

Isothermal jar tests in the range 4 – 44 °C were performed with produced water from the Delaware Basin in Texas using iron chloride as the primary coagulant in conjunction with a commercially available anionic polymer. The floc size and settling velocity distributions were measured by digitally analyzing mobile phone videos during their sedimentation in a water column. Optical images were used to determine 2-D floc fractal dimensions. An empirical relationship linking the settling velocity to the average floc size, fractal dimension, and viscosity was derived.

2. MATERIALS AND METHODS

2.1. Produced water characteristics

Produced water was obtained from the Wolfcamp shale of Delaware Basin, which is the western structural subdivision of the Permian Basin, Texas [22]. Samples were acidified to pH 5 prior to shipment to avoid iron precipitation but brought to the target pH for jar testing. Several of its water quality parameters were measured via inductively coupled plasma – mass spectrometry and colorimetry to establish its composition (Table 1). As summarized in Table 1, the produced water was extremely saline (total dissolved solids ~200,000 mg/L) with chloride and sodium as its main components. Correspondingly, it was significantly denser and more viscous than pure water (see Appendix C and Table 1), which can negatively impact flocculation and sedimentation [20, 23]. Iron was measured colorimetrically using the 2,4,6-tripyridyl-s-triazine (TPTZ) reagent [24] after acidification to pH 3 and monitoring the absorbance of the deep blue-purple colored Fe(II)-TPTZ complex at 590 nm (HACH DR6000). The iron concentration was high (40 mg/L) necessitating its removal prior to possible reuse [3]. Concentrations of bromide, iodide, and boron were also high. Note that low molecular weight organic acids including acetic, propionic, butyric, and lactic acid were present, representing potential carbon sources (substrates) for heterotrophic and sulfate reducing bacteria during long-term storage.

Table 1. Physiochemical characteristics of produced water.

Parameter	**Units**	**Value**
pH	-	6.05 ± 0.30
Turbidity	NTU	69.4 ± 1.65
Total suspended solids (TSS)	mg/L	117 ± 0.06
Total dissolved solids (TDS)	mg/L	197,230 ± 670
Specific gravity	-	1.116 ± 0.002
Viscosity	mPa.s	1.40 ± 0.02
Dissolved organic carbon (DOC)	mg/L as C	391 ± 16.90
Chemical oxygen demand (COD)	mg/L	7,125 ± 425
SiO_2	mg/L	20.0 ± 2.01
Li^+	mg/L	34.0 ± 0.52
B (as $B(OH)_3$)	mg/L	156 ± 1.27
Na^+	mg/L	62,780 ± 2,141
Mg^{+2}	mg/L	1,330 ± 68.20
Mn^{+2}	mg/L	1.25 ± 0.13
Al^{+3}	mg/L	0.10 ± 0.01
Ba^{+2}	mg/L	6.3 ± 0.60
K^+	mg/L	940 ± 96.0
Ca^{+2}	mg/L	8,290 ± 190
Total Fe	mg/L	40.5 ± 1.76
Sr^{+2}	mg/L	822 ± 27.0
NH_4^+	mg/L	1242 ± 65.0
Cl^-	mg/L	133,750 ± 11,250
Br^-	mg/L	1160 ± 59.0
SO_4^{-2}	mg/L	380 ± 25.0
HCO_3^-	mg/L	140 ± 3.20
I^-	mg/L	83 ± 8.20
CH_3COOH	mg/L	156 ± 5.00
C_2H_5COOH	mg/L	3.60 ± 0.04
C_3H_7COOH	mg/L	7.00 ± 0.80
$C_3H_6O_3$	mg/L	12.0 ± 1.00

2.2. Chemical coagulation

Our initial approach was to attempt to use the dissolved iron inherently present in the produced water as the primary coagulant. To this end, free chlorine was added (targeting a 2 mg/L residual at the end of jar testing) for Fe(II) oxidation and the pH was simultaneously increased to 7.5 to facilitate ferric iron precipitation. However, these experimental conditions caused floc-flotation and poor turbidity removal necessitating a different approach. During this preliminary phase of experimentation, various iron dosages (20, 50, 70 and 120 mg/L as Fe) and three pH values (7.5, 8.0 and 8.5) were evaluated while retaining the 2 mg/L free chlorine residual. Maximum turbidity removal was obtained at the highest added iron concentration (120 mg/L) and pH 8.5.

Based on the initial testing, all future jar tests reported in this thesis were performed using 1L of produced water using the optimal values of the primary iron coagulant dosage (120 mg/L of $FeCl_3$ as Fe), pH (8.5 ± 0.1), and a free chlorine dosage of 49 mg/L to achieve residual chlorine concentration of approx. 2 mg/L (actual value of 1.8 ± 0.3 mg/L) in order to combat biological growth. Samples were rapidly mixed at 586 s^{-1} for 2 minutes after which a commercially available linear, anionic polymer of medium molecular weight (FLOPAM EM 235, SNF, Dallas, TX) was added. Note that this product was recommended by our industrial partner. Several dilutions of the as received polymer stock (0, 0.01, 0.05, 0.10 and 0.20% v/v) were evaluated and reported in this thesis. Since its original stock concentration was 1,000 ppm, therefore a 0.10% v/v dose in this thesis corresponds to actual concentration of 1 ppm.

Flocculation was performed at 28 s^{-1} for 10 minutes and flocs were allowed to settle for 10 minutes. Isothermal experiments were performed at 4 °C, 14 °C, 22 °C, 34 °C and 44 °C with 0.10% v/v polymer dose (Innova 42 incubator, Eppendorf). The temperature of the suspension was monitored continuously using a probe connected to a meter (LDO101 and HQ430d, HACH). Temperature profiles during experimentation are summarized in APPENDIX B. At the end of each experiment around 100 mL of the supernatant was pipetted for water quality analysis.

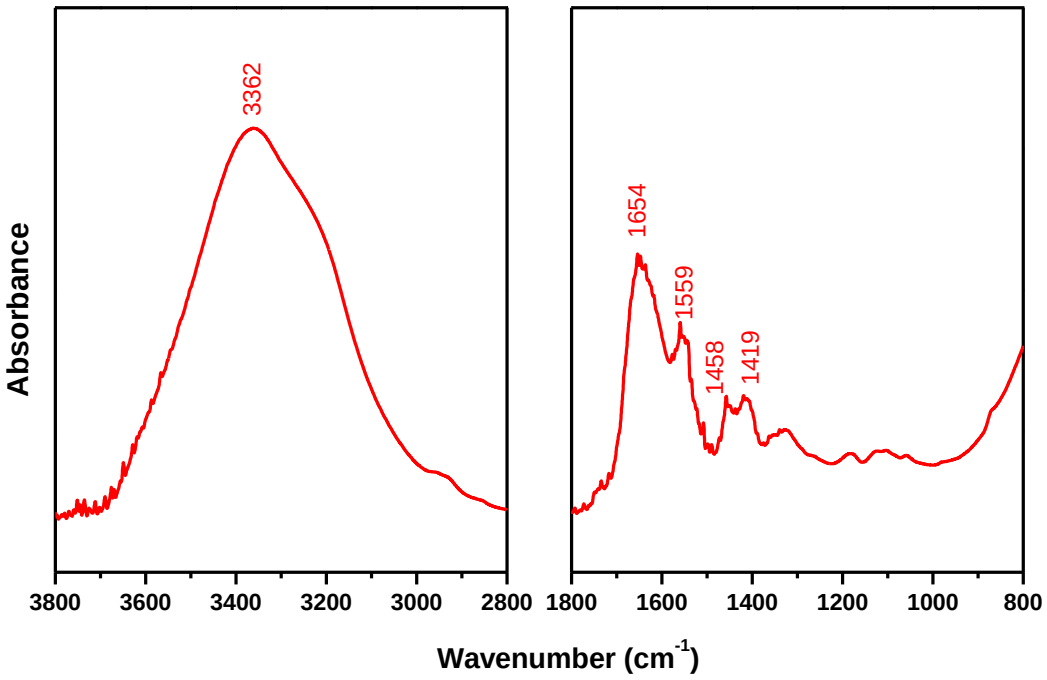

Figure 1. ATR-FTIR spectrum of polymer.

The ATR-FTIR spectrum (Figure 1) of the air-dried polymer exhibited the following peaks: 1419 cm^{-1} corresponding to v_sCOO- of Na-acrylate / υ CN of acrylamide, 1559 cm^{-1} which corresponds to v_{as}COO- of Na-acrylate, 1654 cm^{-1}

corresponding to vC=O of acrylamide, and δ OH of water. The broad bands at 3700–3000 cm^{-1} (vH−O−H) are largely due to residual water which overwhelmed any amine peaks (v_{as} and v_s NH_2 of acrylamide). These validate the composition of the FLOPAM EM 235 polymer as designated by the manufacturer (i.e. poly(sodium acrylate-*co*-acrylamide)) [25].

2.3. Fractal dimension

The box-counting technique was used to determine 2D fractal dimension ($D_{f,2d}$) of flocs after imaging them on an Olympus BX53 optical microscope in bright field transmittance mode. All images were taken using only a 4X objective lens so as to image the entire floc structure. The z-axis motor drive installation and cellSens Dimension software facilitated easy acquisition and processing of high-quality images. As shown in Figure 2, the technique involves overlaying the image with squares of decreasing sizes (of length r) and determining the number of squares (N) that fully contain the floc [26-28]. A logarithmic plot of number of squares occupied and size of squares gives $D_{f,2d}$ (equations 1 and 2). A minimum of 50 flocs were analyzed in each experiment using a program written in MATLAB.

$$D_{f,2d} = \lim_{r \to 0} \frac{Log\,(N)}{Log(\frac{1}{r})} \tag{1}$$

$$log(N) = D_{f,2d} \left(\frac{1}{r}\right) + c \tag{2}$$

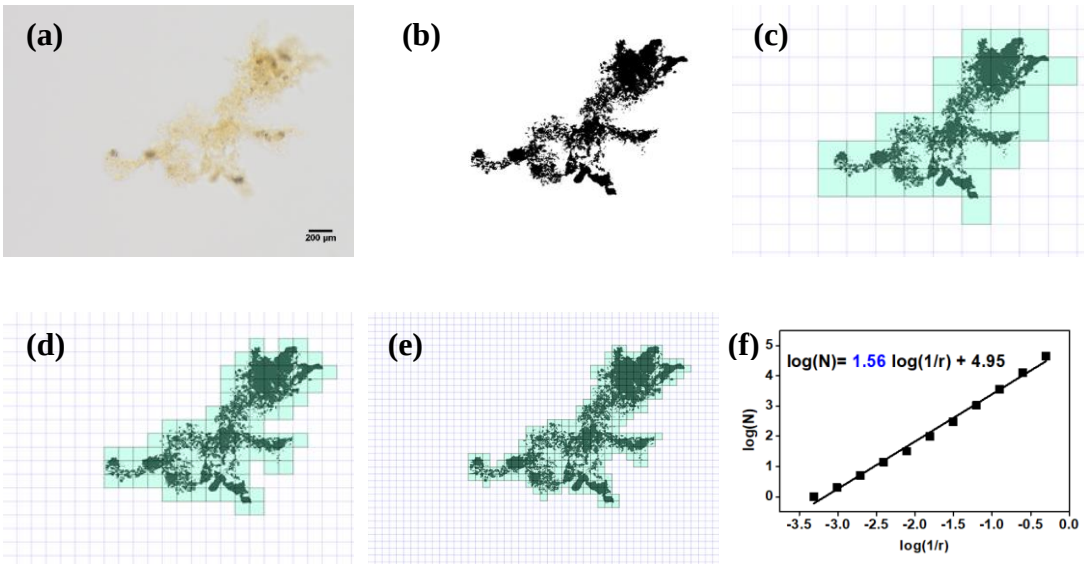

Figure 2. Illustration of box-counting technique. (a) microscopic image of floc (scale bar = 200 µm), (b) binary image generated after thresholding, (c) to (f) implementation and data analysis.

2.4. Floc size and settling velocity

Figure 3 is a schematic representation of the experimental setup used to determine the size and settling velocity of the flocs. Sedimentation columns were set up with a height of 40 cm and width of 6 cm. At the completion of a jar test, flocs were carefully extracted using a 10 ml pipette with its tip cut to avoid breakage to the extent possible and transferred to the settling column containing clear supernatant from the jar test to maintain identical physicochemical fluid properties (e.g. density, viscosity, and ion concentration). The column was backlit by an LED light and a video of settling flocs was recorded using a cellphone camera at 60 fps and 1080 x 1920 pixels resolution.

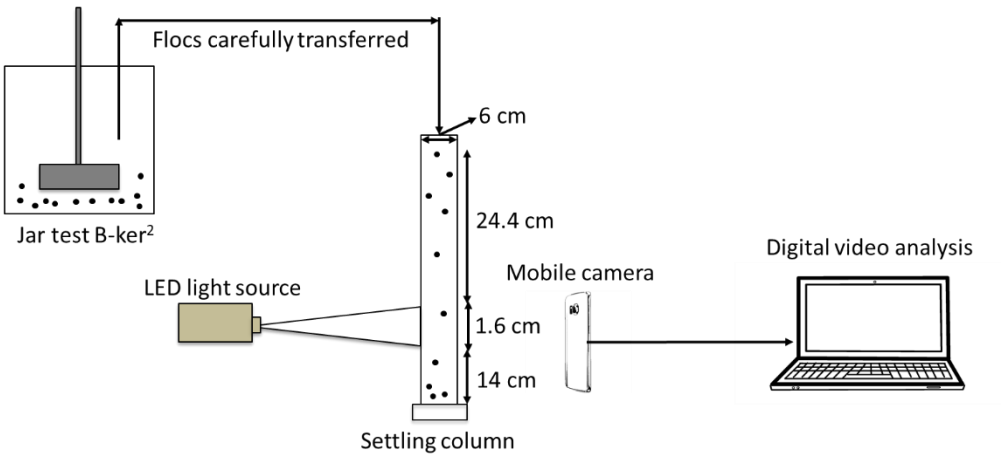

Figure 3. Schematic diagram of the experimental setup used to determine the size and settling velocity.

A MATLAB code was developed to process the video and to measure the size and settling velocity of flocs using the technique similar to Kelley and Ouellette [29]. The video was split into frames and the threshold pixel value was set in each case to differentiate the flocs from the background and clearly visualize their settling. The Image Processing Toolbox™ in MATLAB was used to capture the flocs and measure their area, which was then converted to an equivalent spherical diameter as shown in Figure 4.

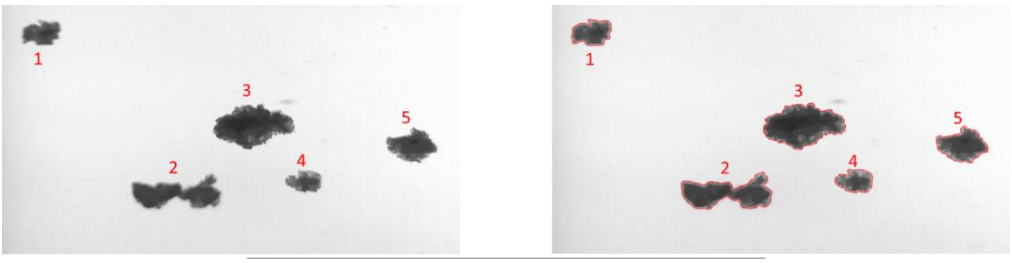

Floc	Area (mm^2)	Equivalent diameter (mm)
1	3.06	1.97
2	7.45	3.08
3	9.31	3.44
4	2.54	1.80
5	4.53	2.40

Figure 4. Illustration of particle capture and size determination.

Particle tracking velocimetry (PTV) which employs a Lagrangian approach to follow each floc, was used to track aggregates in each frame and measure their settling velocity. The vertical displacement of the center of mass of each floc between frames and the duration of frames were used to calculate sedimentation rate. Around 500 flocs were analyzed in each experiment to obtain floc size and settling velocity distributions [23].

Based on preliminary tests the video was taken at an optimum height of approx. 14 cm from the bottom and 24 cm from the top of the settling column after particles attained and maintained their terminal velocity. In the video frames, a central investigation window of 2 cm x 1.6 cm was chosen for analysis to minimize wall effects. MATLAB data were processed using Python to discard any size and settling velocity measurements with a coefficient of variance greater than 0.3 so as to remove the measurements of particles that were under the influence of any wall effects in the direction normal to the video frame and of those not maintaining terminal velocity

during capture. These quality control measures ensure precise and accurate measurement of floc size and sedimentation rate as further described in APPENDIX A.

2.5. Scanning electron microscopy

Aggregate morphology was also visualized via high-resolution scanning electron microscopy (VEGA3, TESCAN). Flocs were carefully extracted using a 10 ml pipette with the tip cut to reduce breakage and gently washed with ultrapure water. A drop of this washed floc suspension was then pipetted onto carbon taped aluminum SEM stubs and left to air dry, sputter coated with 10 nm gold (Sputter Coater 108auto, Cressington), and imaged at a 20 kV acceleration voltage.

2.6. Zeta potential

The electrophoretic mobility of colloids present in the produced water and from each jar testing experiment was measured using electrophoretic light scattering (Anton Paar Litesizer™ 500) and converted into a zeta potential using the Helmholtz-Smoluchowski equation [30, 31]. A standard latex reference material with zeta potential of -42.0 (± 4) mV was used to ensure measurement credibility.

2.7. Viscosity

The absolute viscosity of produced water and polymer solution were probed using a Thermo Scientific™ HAAKE™ MARS™ 60 rheometer. The shear rate was increased from 0.1 to 1,000 s^{-1} and then decreased back to the starting shear rate in a stepwise fashion (collecting 5 data points per decade of shear rate) using a double-gap concentric cylinder measuring geometry. The temperature was adjusted to target

values of 4, 11, 20, 22, 34, 44, and 60 °C using a Peltier module with ± 0.1 °C precision. Inertia effects were limited by waiting 10 seconds before logging the data at each shear rate step. Using a polyoxymethylene hood and solvent trap reduced sample evaporation. The measured viscosity was then plotted as a function of shear rate for each temperature.

2.8. Hydrodynamic size

Dynamic light scattering (DLS) was performed using Zetasizer Nano ZS (Malvern) to measure the hydrodynamic size of the polymer subunits in the range 4 °C to 60 °C. The polymer was diluted in a 1:10 ratio using 10 mM KNO_3 to increase the inter-particle spacing so as to minimize polymer molecule interactions [21]. An equilibration time of 10 minutes was chosen for each 5 °C step and an average of three measurements are reported.

2.9. ATR-FTIR

ATR-FTIR spectra were collected for the air-dried polymer using a Nicolet™ iS10 spectrometer equipped with Ever-Glo source, DTGS detector, KBr beam splitter and Omnic 9.0 software in the range of 4000 – 600 cm^{-1} in ATR mode using a diamond iTX accessory. Prior to each analysis, the background spectrum was collected and an average of three separate spectra, each consisting of 128 scans at 4 cm^{-1} resolution are reported herein.

3. RESULTS AND DISCUSSION

3.1. Optimization of polymer dosage at room temperature

3.1.1. Polymer effect on floc size and morphology at 22 °C

Optical images of the flocs obtained from jar tests at 22 °C with different polymer concentrations showed that addition of the coagulant aid substantially increased the floc size (Figure 5). Higher exposure times of same light intensity were needed to image flocs generated with high polymer concentrations, which relates to formation of closely packed flocs at high dosages.

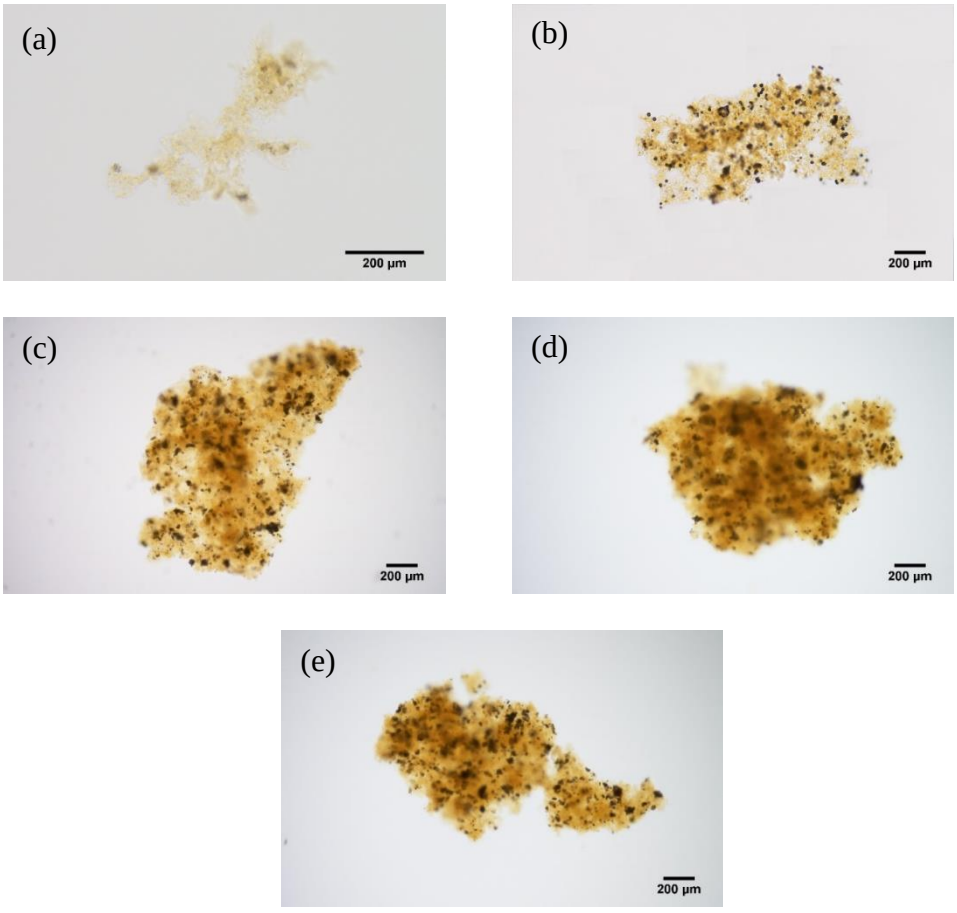

Figure 5. Optical images of representative flocs produced from room temperature jar tests with (a) no polymer, i.e. only 120 mg/L $FeCl_3$ as Fe, (b) 0.01% v/v polymer, (c) 0.05% v/v polymer, (d) 0.10% v/v polymer, and (e) 0.20% v/v polymer.

Equivalent floc diameters obtained using the technique outlined in section 2.4 are shown in Figure 6. As seen, polymer addition enhanced destabilization by forming bigger flocs and shifting size distributions to the right, even as large as 10 mm at the highest dose (0.2% v/v). Importantly, the biggest enhancements in the average size were obtained at lowest polymer doses; rising from 180 μm when no polymer was added to 540 μm for 0.01% v/v dose and further to 830 μm for a 0.05% v/v dosage. Adding more polymer, did not appreciably increase the average floc size (only 890 μm at 0.1% and 1,000μm at 0.2% v/v).

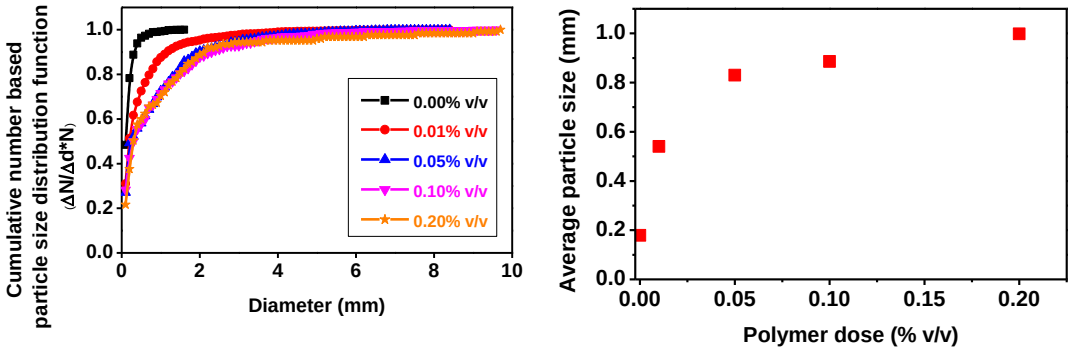

Figure 6. Increase of floc size with polymer dose showing floc size distribution (left panel) and average floc size (right panel) for different polymer doses.

Qualitative inspection of images in Figure 5 also reveals that flocs were loose, open, and porous at low polymer doses (< 0.1% v/v) whereas closer, more densely-packed structures were visualized at doses ≥ 0.1% v/v. This was quantified by digital analysis of a minimum of 50 images (similar to Figure 5) using the box counting technique outlined in section 2.3, which showed that flocs' 2D fractal dimension ($D_{f,2d}$) increased for any polymer dose (Figure 7). As observed, $D_{f,2d}$ increased from 1.44

when only iron was employed for coagulation to 1.74 at the highest polymer dose evaluated.

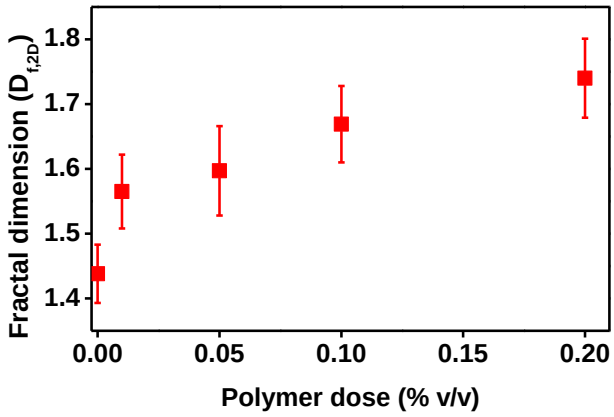

Figure 7. Increasing fractal dimension with polymer addition.

SEM images also show changes in surface morphology of the flocs with polymer addition as summarized in Figure 8. In the case of no polymer, floc surfaces appeared to be smooth and gelatinous (Figure 8a) with no discernable order or habit consistent with the precipitation of polymorphic amorphous $Fe(OH)_3$ possibly arising from competition of organic acids (see Table 1) with hydroxyl ions. At high doses, flocs appeared to be rough as a combination of individual aggregates held together by the polymer (e.g. Figure 8d and e).

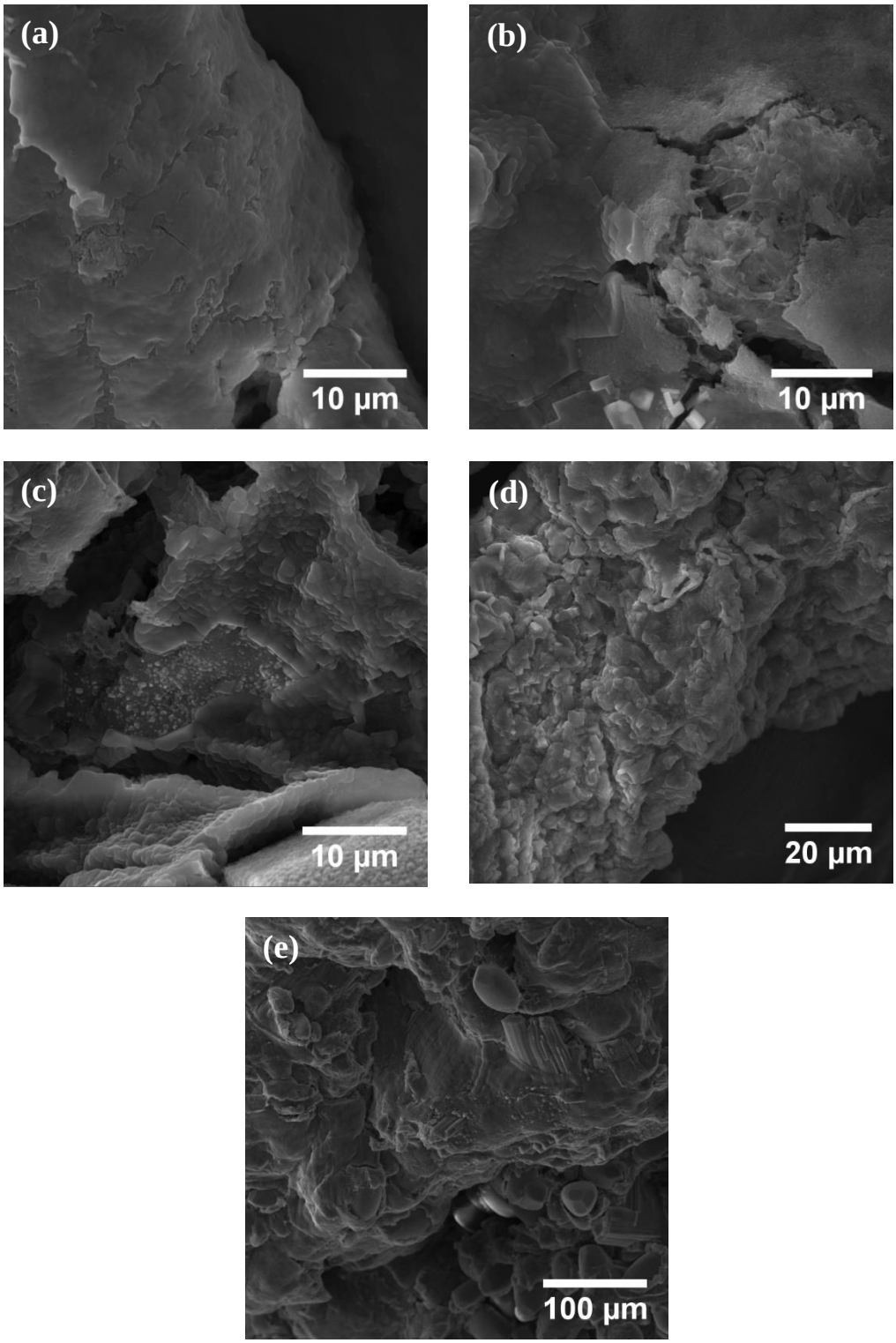

Figure 8. SEM images of representative flocs produced from room temperature jar tests with (a) no polymer, (b) 0.01% v/v polymer, (c) 0.05% v/v polymer, (d) 0.10% v/v polymer, and (e) 0.20% v/v polymer.

3.1.2. Polymer effects on settling velocity

Sedimentation videos were digitally analyzed to measure the settling velocities of flocs as described in section 2.4. As summarized in Figure 9, the average sedimentation rate increased monotonically over the entire range of polymer dosages. In other words, significant improvements in sedimentation rates from 4.6 to 5.8 mm/s were measured even at the highest polymer doses 0.1 and 0.2% v/v unlike floc size, which appeared to reach an asymptotic value around a dosage of 0.05% v/v (see Figure 6). This is attributed to the considerable increase in fractal dimensions at high polymer doses (1.60, 1.67, and 1.74, at dosages of 0.05, 0.1, and 0.2% v/v in Figure 7), emphasizing the importance of floc morphology in its settling rate.

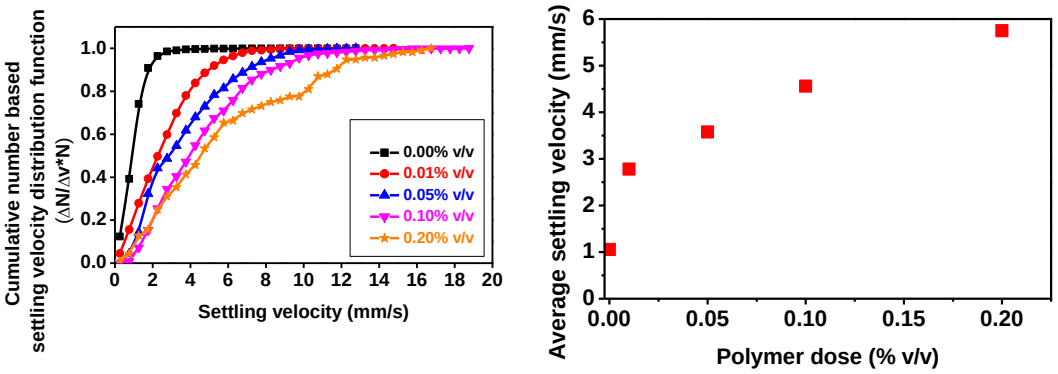

Figure 9. Increase of settling velocity with polymer dose showing settling velocity distribution (left panel) and average settling velocity (right panel) for different polymer doses.

3.1.3. Iron and turbidity removal

In all cases, ≥ ~90% of iron and turbidity were removed demonstrating the feasibility of this approach to their control before potentially reusing produced water. The supernatant water quality was similar for the two highest polymer dosages investigated reaching ≥ 97% turbidity and iron removal. Considering polymer cost

and only minimal improvements at a higher dose (0.2% v/v), a concentration of 0.1% v/v was chosen to be "optimum" and used to investigate temperature effects on performance.

Table 2. Summary of total iron and turbidity and their removals.

Polymer dosage (% v/v)	Supernatant turbidity (NTU)	Turbidity removal (%)	Supernatant total iron (mg/L)	Total iron removal (%)
0.00	5.23	94.1	4.39	89.0
0.01	4.20	95.2	3.77	90.6
0.05	3.83	95.7	2.98	92.6
0.10	1.90	97.8	1.22	97.0
0.20	1.80	97.8	1.07	97.3

3.1.4. Floc destabilization mechanisms

The ζ potential of colloids present in the raw produced water was near neutral (represented as a blue dot "●" in Figure 10) owing to its high ionic strength and presence of high concentrations of multivalent cations (e.g. Mg, Ca, Fe). Adding 120 mg/L $FeCl_3$ as coagulant reversed particle charge, potentially due to adsorption of positively charged hydrolyzed iron species. This suggests that sweep coagulation was the dominant destabilization mechanism since turbidity was successfully removed even though colloids had a substantially positive ζ potential (+15 mV). This also justified the use of an anionic polymer as a coagulant aid, which as expected, reduced the ζ potentialupon progressive addition. Note that floc sizes significantly increased in Figure 6 for dosages ≥ 0.05% v/v corresponding to (slightly) negative ζ potential conditions (Figure 10). This indicates that polymer adsorption was dominated by non-electrostatic interactions, probably facilitated by the low diffuse layer thickness arising

from the the high salinity of the produced water, and that interparticle bridging was the dominant destabilization mechanism. Another possibility is the formation of particle-(Mg or Ca)-polyelectrolyte bridges given their high concentrations in the produced water [32].

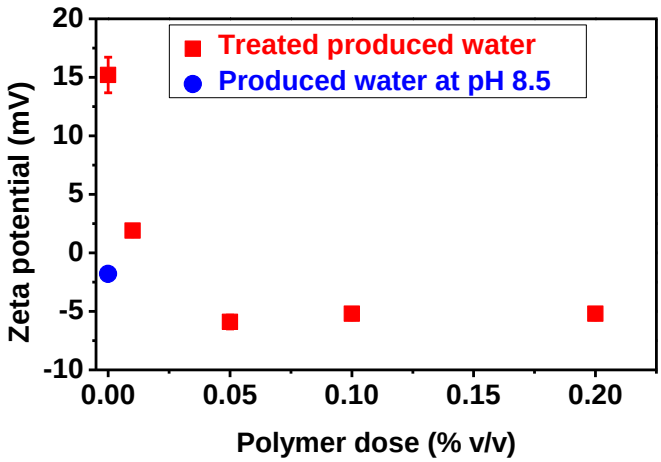

Figure 10. Zeta potential of produced water and supernatants from jar test.

3.2. Temperature effects on coagulation/flocculation

3.2.1. Effect on flocs size and morphology

As summarized in Figure 11 right panel, flocs were biggest on average (~ 900 µm) at room temperature. Both increasing and decreasing temperature reduced average floc size considerably, for example to 240 µm at 4 °C and 380 µm at 44 °C. Additionally, the entire distribution shifted to smaller sizes for values other than room temperature (Figure 11 left panel).

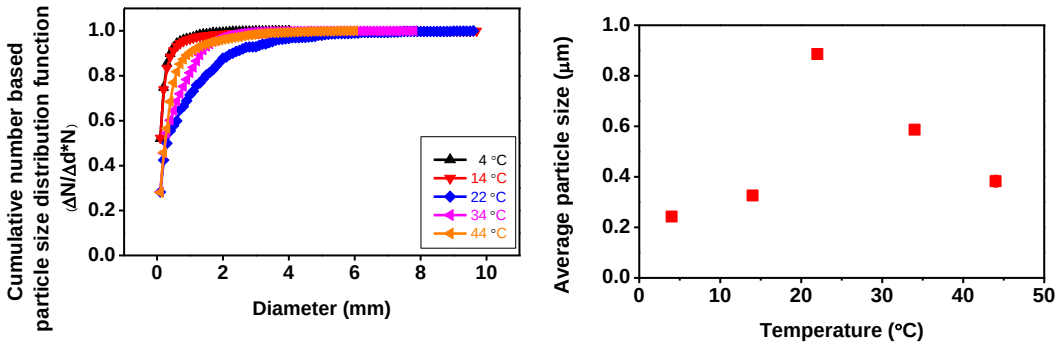

Figure 11. Floc sizes changed when temperature changed from 22 °C. The entire cumulative distribution is given in the left panel and the average size is shown in the right panel for different temperatures.

These measurements were supported by optical images (Figure 12) which spotted considerably smaller flocs at all temperatures other than 22 °C. Figure 12 also qualitatively shows that floc morphology was modified by temperature changes with denser structures visible at room temperature. In contrast, flocs appeared to be looser and open at temperatures both lower and higher than 22 °C.

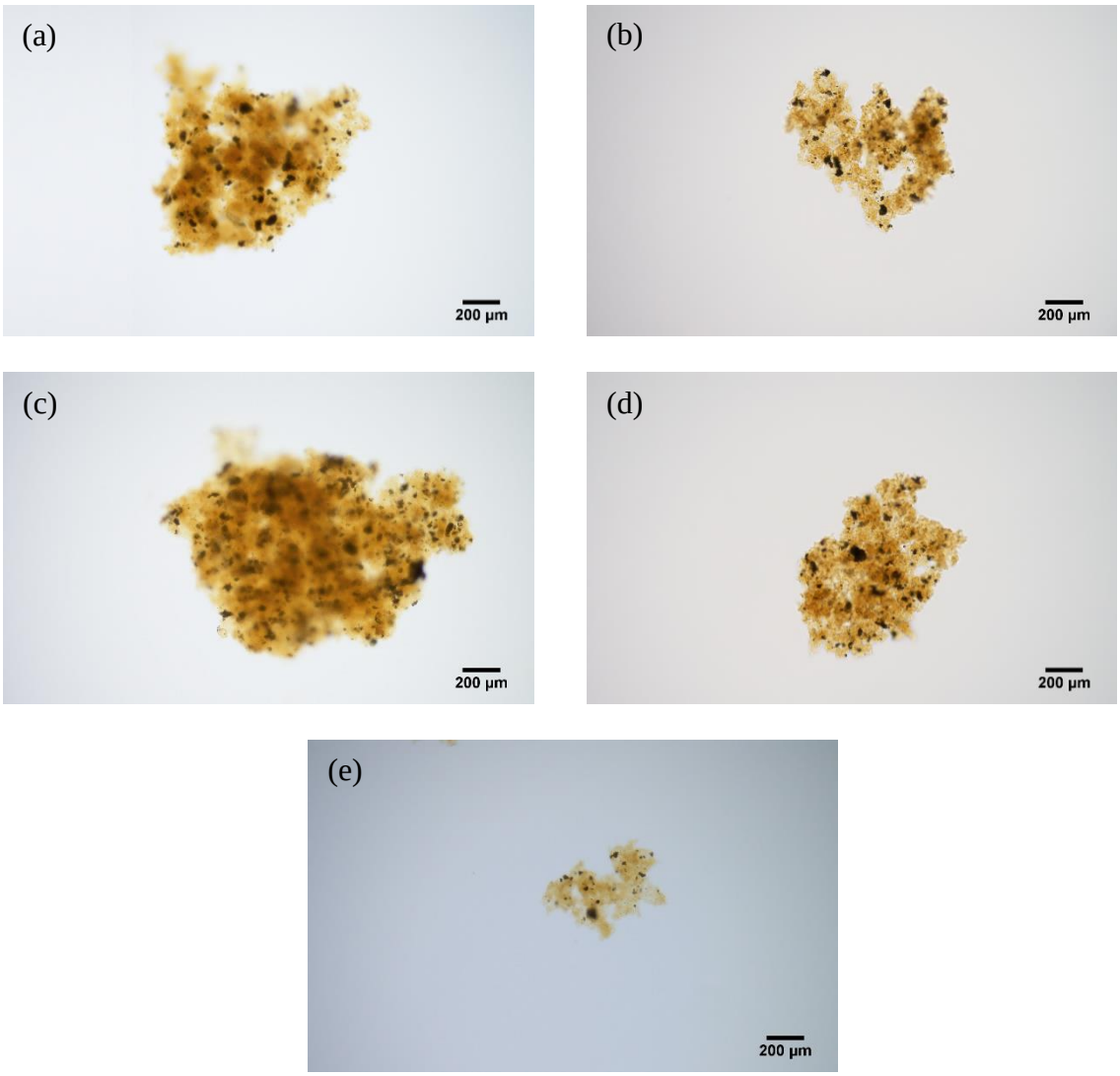

Figure 12. Optical images of representative flocs produced from jar tests performed at (a) 4 °C, (b) 14 °C, (c) 22 °C, (d) 34 °C, and (e) 44 °C with 120 mg/L (as Fe) $FeCl_3$ and 0.1% v/v polymer.

These observations were confirmed by quantitative digital analysis of optical images for 2D fractal dimensions by box counting. As summarized in Figure 13, flocs exhibited the highest fractal dimension at room temperature (~ 1.67) decreasing to ~ 1.58 at the highest (44 °C) and lowest temperatures (4 °C) investigated.

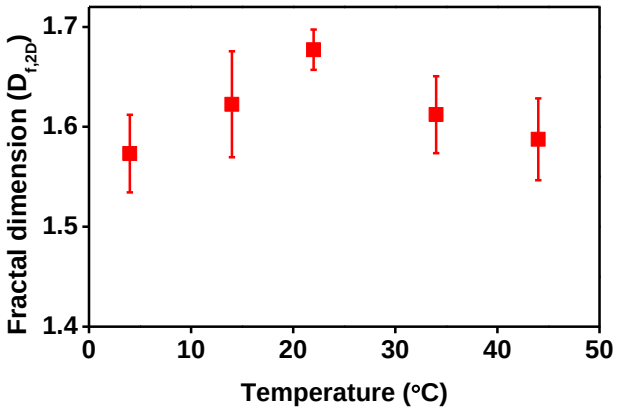

Figure 13. Decreasing fractal dimension at temperatures other than 22 °C.

3.2.2. Viscosity and hydrodynamic size of polymer

The polymer viscosity and its hydrodynamic size were measured to better understand their role in aggregation. As summarized in Figure 14, the polymer employed in this research exhibited shear thinning behavior. Also as expected, its viscosity decreased with increasing temperature with a zero-shear viscosity of 60.7 mPa.s at 4 °C compared with only 18.4 mPa.s at 44 °C. Decreasing viscosities at temperatures above 22 °C have been reported to negatively impact polymeric flocculation by disrupting hydrogen bonds between the polymer and water in-turn favoring polymer-polymer interactions leading to more coiling [21] reducing their ability to form bridges between colloids during flocculation. To our knowledge, polymer behavior at lower temperatures (< 22 °C) during wastewater treatment are not available in the peer-reviewed literature.

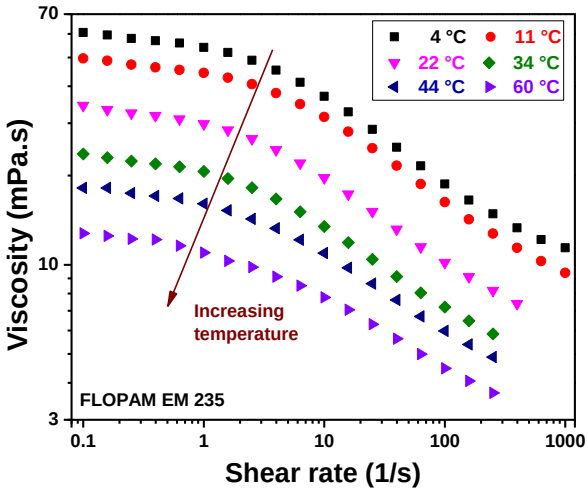

Figure 14. Decreasing viscosity of polymeric flocculent aid with increasing temperature and shear rate.

Dynamic light scattering confirmed decreasing polymer hydrodynamic sizes above room temperature (e.g. 340 µm at 22 °C and 240 µm at 44 °C) as shown in Figure 15, impeding its ability to effectively perform bridging flocculation in warm waters. Similar results have been reported for a Na-acrylate carboxyl-substituted anionic polyacrylamide copolymer flocculent aid [21]. Note that the reduction in size was not as dramatic for temperatures < 22 °C, reaching 290 µm at 4 °C (only a 15% drop). Nevertheless, this hindered aggregation at low temperatures as shown in Figure 11.

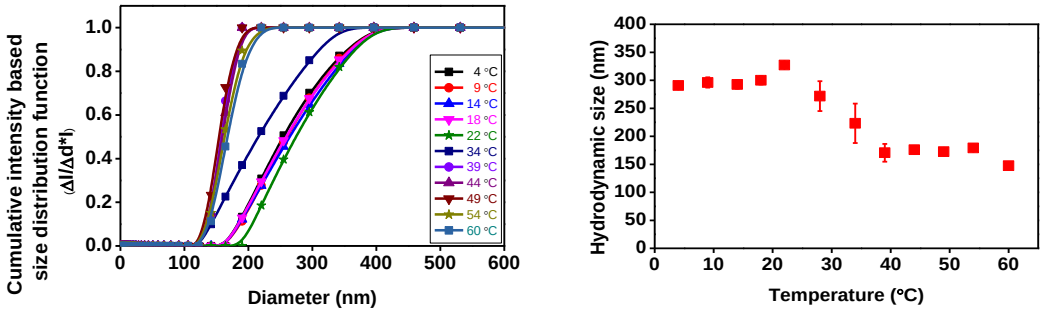

Figure 15. Differences in hydrodynamic size with temperature. The left panel shows the entire intensity-based distribution and the right panel shows the average size.

3.2.3. Temperature effects on settling velocity

Flocs' settling velocity followed the identical trend as their size and fractal dimension in that highest values were measured at room temperature whereas sedimentation rate was retarded both at higher and lower temperatures (Figure 16). The maximum sedimentation rate was 4.5 mm/s at 22 °C, which decreased to 1.1 mm/s at 4 °C and to 3.1 mm/s at 44 °C. The size effect for free settling (Type 1) is consistent with Stokes' law, which predicts a nonlinear dependence for impermeable spheres in the absence of inertial and boundary effects. Since the suspending fluid permeates porous flocs, with higher fluid collection efficiencies calculated for more permeable flocs (i.e. low $D_{f,2D}$), the drag experienced by them during settling is inversely related to their fractal dimension [33]. In other words, loose, open flocs (low $D_{f,2D}$) are expected to settle slower than their denser counterparts having the same overall size [34].

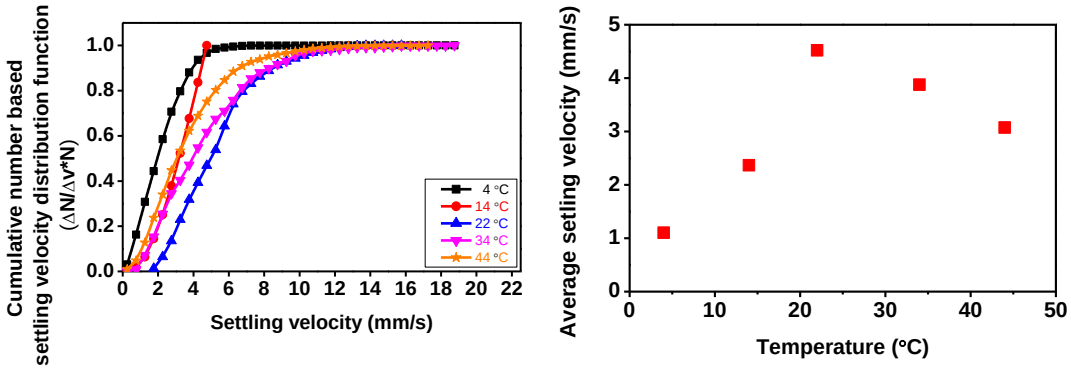

Figure 16. Decreasing settling velocity for temperatures other than 22 °C. The entire settling velocity distribution (left panel) and average settling velocity (right panel) at different temperatures are shown.

In addition to floc size and density (i.e. $D_{f,2D}$), the suspension viscosity also influences their sedimentation [23]. Settling rates during wastewater treatment have

been reported to increase with temperature since lower viscosities reduce the frictional resistance to sedimentation with an opposite trend at lower temperatures due to increasing viscosity [20]. As shown in Figure 17, the viscosity of the produced water averaged 1.27 mPa.s at 22 °C, expectedly increasing to 2.1 mPa.s at 4 °C and reducing to 0.85 mPa.s at 44 °C. Several authors have also reported a linear inverse relationship between the absolute viscosity of the suspending medium and fractal floc settling velocity e.g. [35, 36].

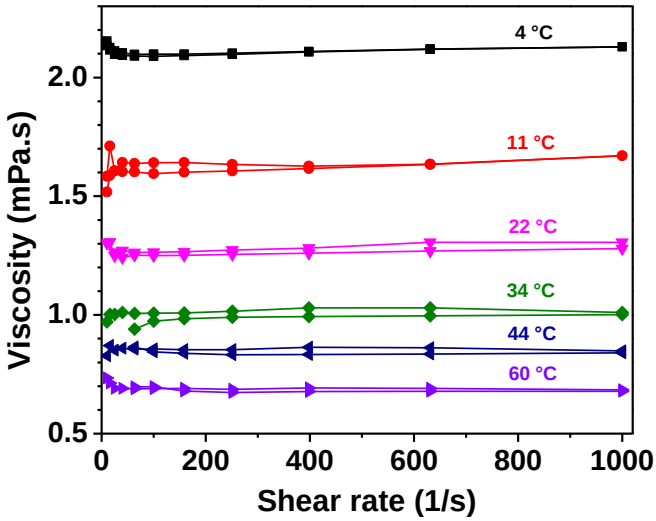

Figure 17. Decreasing viscosity of produced water sample with increasing temperature.

Theoretical models for the sedimentation rate of coagulated aggregates are typically derived using numerous idealizations. These generally include (i) an initially monodispersed suspension of identical primary colloids, (ii) both primary particles and the flocs are perfectly spherical, (iii) a prescribed model for flow internal to the porous floc (e.g. Brinkman or Darcy), (iv) the effective density of the floc is known or can be calculated, (v) the fractal dimension does not vary with floc size, and so on [34-38].

Even though these assumptions are not satisfied in water and wastewater treatment practice, the settling velocity ($V_{settling}$) of aggregates typically scales in a power law fashion with floc diameter (D) and the 3-dimensional fractal dimension ($D_{f,3D}$) and inversely with absolute viscosity (μ):

$$V_{\text{settling}} \propto \frac{D^{(D_{f,3D}-1)}}{\mu} \tag{3}$$

Since in this work only the 2-D fractal dimension ($D_{f,2D}$) was measured, the following empirical relationship was evaluated where the parameter "a" was estimated by fitting Equation 4 to experimental data:

$$V_{\text{settling}} \propto \frac{D^{(D_{f,2D}-a)}}{\mu} \tag{4}$$

As shown in Figure 18, this model accurately captured the entire dataset with the parameter "a" equaling 1.5. The physical interpretation of this value is not clear although it is heartening to note that only a single fitting parameter was necessary to quantitatively interpret the entire temperature range and that it was an improper fraction (=3/2).

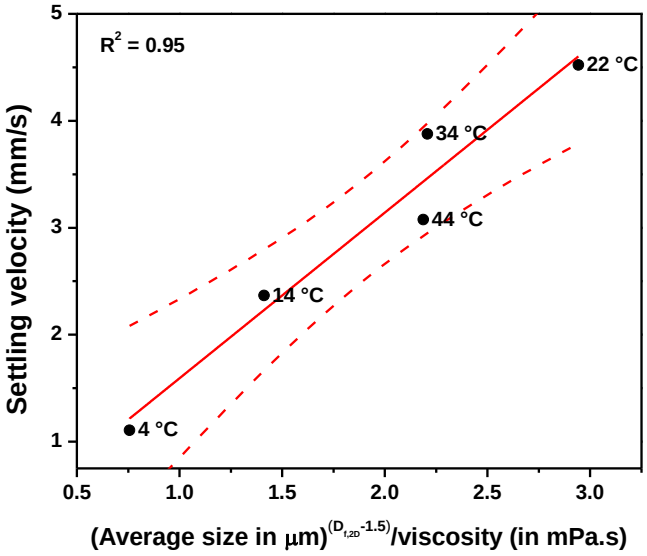

Figure 18. Empirical determination of a fractal sedimentation model for flocs formed at various temperatures. The solid line is the best-fit and dashed lines show the 95% confidence intervals.

3.2.4. Temperature effects on supernatant water quality

As summarized in Table 3, suspended solids and iron were very-well removed in all cases with supernatant turbidity < 2 NTU and total iron ≤ 1.2 mg/L demonstrating the applicability of the process under optimized chemical dosages for treating produced water to a level that can be used for further hydraulic fracturing over the entire temperature range investigated. Small differences in removals are attributed to errors associated with accurately modifying the paddle angular velocity to maintain the same average flocculation shear rate (i.e. the G value) at different temperatures, manual measurements of low levels of turbidity and iron, and experimental noise.

Table 3. Summary of jar tests performed at different temperatures.

Temperature (˚C)	**Supernatant turbidity (NTU)**	**Turbidity removal (%)**	**Supernatant total iron (mg/L)**	**Total iron removal (%)**
4	0.76	99.1	0.32	99.2
14	0.50	99.4	0.19	99.5
22	1.90	97.8	1.2	97.0
34	0.47	99.5	0.25	99.4
44	0.29	99.7	0.19	99.5

4. CONCLUSIONS

- Adding a polymeric coagulant aid dramatically increased floc sizes and sedimentation rates compared with using a hydrolyzing metal-ion coagulant ($FeCl_3$) alone (e.g. from 180 μm to 540 μm and from 1.06 mm/s to 2.78 mm/s respectively at room temperature). This information can be employed to design high rate clarifiers for oil-field applications.
- Settling velocities of coagulated aggregates conformed to a power law model incorporating its average size and 2-D fractal dimension and inversely with viscosity over the entire range of temperatures investigated (4 – 44 °C).
- Employing a polymeric coagulant aid in conjunction with $FeCl_3$ as the primary coagulant and oxidation with free chlorine removed ≥ 98% turbidity (suspended solids) and ≥ 97% iron (as Fe(III)) from produced water obtained from the Permian Basin through a combination of sweep coagulation and adsorption and inter-particle bridging.
- Coagulation-flocculation-sedimentation is a highly effective and facile method for produced water reuse in hydraulic fracturing over the entire environmentally relevant temperature range.
- Although laboratory-scale jar tests provided chemical dosing and data for process design (in addition to insights into underlying mechanisms), careful consideration needs to be given for scale-up and field-scale performance evaluation before recommendations can be made for implementation.

REFERENCES

1. Scanlon, B.R., R.C. Reedy, F. Male, and M. Walsh, *Water issues related to transitioning from conventional to unconventional oil production in the Permian Basin.* Environmental Science & Technology, 2017. **51**(18): p. 10903-10912.
2. Kondash, A.J., N.E. Lauer, and A. Vengosh, *The intensification of the water footprint of hydraulic fracturing.* Science Advances, 2018. **4**(8): p. eaar5982.
3. Walsh, J. and R. Sharma, *Fit-for-purpose water treatment in Permian Shale – Field data, lab data and comprehensive overview.* SPE International, 2018. **SPE 191529**.
4. Veil, J., *U.S. produced water volumes and management practices in 2012*. 2015: Water Protection Council.
5. Davies, R., G. Foulger, A. Bindley, and P. Styles, *Induced seismicity and hydraulic fracturing for the recovery of hydrocarbons.* Marine and Petroleum Geology, 2013. **45**: p. 171-185.
6. Sharma, R., K. McLin, K. Bjornen, A. Shields, Z. Hirani, and S. Adham, *Fit-for-purpose treatment of produced water for hydraulic fracturing – A Permian Basin experience.* International Petroleum Technology Conference, 2015: p. IPTC 18340.
7. McLin, K.S., J.M. Freeman, S. Aarekol, E.S. McKean, R.R. Sharma, J. Rincon, and J. Speaker, *Permian unconventional water Management: Collaboration to develop full cycle solutions.* SPE International, 2015. **SPE 174538**.

8. CH2MHILL, *U.S. onshore unconventional exploration and production water management case studies.* Energy Water Initiative, 2015.

9. Ye, X., N. Tonmukayakul, P. Lord, and R. Lebas, *Effects of total suspended solids on permeability of proppant pack.* SPE International, 2013. **SPE 165085**.

10. Sharma, R.R. and K. Bjornen, *Systematic approach for developing a "fit-for-purpose" treatment for produced water reuse in hydraulic fracturing.* Unconventional Resources Technology Conference, 2018. **URTeC 2902544**.

11. Fakhru'l-Razi, A., A. Pendashteh, L.C. Abdullah, D.R. Biak, S.S. Madaeni, and Z.Z. Abidin, *Review of technologies for oil and gas produced water treatment.* Journal of Hazardous Materials, 2009. **170**(2-3): p. 530-51.

12. Chorghe, D., M.A. Sari, and S. Chellam, *Boron removal from hydraulic fracturing wastewater by aluminum and iron coagulation: Mechanisms and limitations.* Water Research, 2017. **126**: p. 481-487.

13. Sari, M.A. and S. Chellam, *Mechanisms of boron removal from hydraulic fracturing wastewater by aluminum electrocoagulation.* Journal of Colloid and Interface Science, 2015. **458**: p. 103-11.

14. Gregory, J. and S. Barany, *Adsorption and flocculation by polymers and polymer mixtures.* Advances in Colloid and Interface Science, 2011. **169**(1): p. 1-12.

15. Jarvis, P., B. Jefferson, J. Gregory, and S.A. Parsons, *A review of floc strength and breakage.* Water Research, 2005. **39**(14): p. 3121-37.

16. Rosenblum, J.S., K.A. Sitterley, E.M. Thurman, I. Ferrer, and K.G. Linden, *Hydraulic fracturing wastewater treatment by coagulation-adsorption for removal of organic compounds and turbidity.* Journal of Environmental Chemical Engineering, 2016. **4**(2): p. 1978-1984.

17. Camarillo, M.K., J.K. Domen, and W.T. Stringfellow, *Physical-chemical evaluation of hydraulic fracturing chemicals in the context of produced water treatment.* Journal of Environmental Management, 2016. **183**: p. 164-174.

18. Lester, Y., I. Ferrer, E.M. Thurman, K.A. Sitterley, J.A. Korak, G. Aiken, and K.G. Linden, *Characterization of hydraulic fracturing flowback water in Colorado: implications for water treatment.* Science of the Total Environment, 2015. **512-513**: p. 637-644.

19. Hogg, R., *The role of polymer adsorption kinetics in flocculation.* Colloids and Surfaces A: Physicochemical and Engineering Aspects, 1999. **146**(1): p. 253-263.

20. Winkler, M.K., J.P. Bassin, R. Kleerebezem, R.G. van der Lans, and M.C. van Loosdrecht, *Temperature and salt effects on settling velocity in granular sludge technology.* Water Research, 2012. **46**(12): p. 3897-902.

21. Mpofu, P., J. Addai-Mensah, and J. Ralston, *Temperature influence of nonionic polyethylene oxide and anionic polyacrylamide on flocculation and dewatering behavior of kaolinite dispersions.* Journal of Colloid and Interface Science, 2004. **271**(1): p. 145-56.

22. Hennenfent, G., M. Hegmann, C. Harris, and K. Schwartz, *From core analysis to log-based pay identification in the Delaware Basin Wolfcamp Formation.* Interpretation, 2015. **3**(3): p. SV35-SV44.

23. Benjamin, M.M. and D.F. Lawler, *Water quality engineering : physical/chemical treatment processes*. 2013: Hoboken, New Jersey : Wiley.

24. Collins, P.F., H. Diehl, and G.F. Smith, *2,4,6-Tripyridyl-s-triazine as reagent for iron. Determination of iron in limestone, silicates, and refractories.* Analytical Chemistry, 1959. **31**(11): p. 1862-1867.

25. Magalhães, A.S.G., M.P. Almeida Neto, M.N. Bezerra, N.M.P.S. Ricardo, and J.P.A. Feitosa, *Application of ftir in the determination of acrylate content in poly(sodium acrylate-co-acrylamide) superabsorbent hydrogels.* Química Nova, 2012. **35**(7): p. 1464-1467.

26. Vahedi, A. and B. Gorczyca, *Application of fractal dimensions to study the structure of flocs formed in lime softening process.* Water Research, 2011. **45**(2): p. 545-56.

27. Landini, G., *Fractals in microscopy.* Journal of Microscopy, 2011. **241**(1): p. 1-8.

28. Gamage, N.P., J.D. Rimer, and S. Chellam, *Improvements in permeate flux by aluminum electroflotation pretreatment during microfiltration of surface water.* Journal of Membrane Science, 2012. **411-412**: p. 45-53.

29. Kelley, D.H. and N.T. Ouellette, *Using particle tracking to measure flow instabilities in an undergraduate laboratory experiment.* American Journal of Physics, 2011. **79**(3): p. 267-273.

30. Sze, A., D. Erickson, L. Ren, and D. Li, *Zeta-potential measurement using the Smoluchowski equation and the slope of the current–time relationship in electroosmotic flow.* Journal of Colloid and Interface Science, 2003. **261**(2): p. 402-410.

31. Hiemenz, P.C. and R. Rajagopalan, *Principles of colloid and surface chemistry. 3rd ed., rev. and expanded.* 1997: New York : Marcel Dekker.

32. Witham, M.I., A.F. Grabsch, A.T. Owen, and P.D. Fawell, *The effect of cations on the activity of anionic polyacrylamide flocculant solutions.* International Journal of Mineral Processing, 2012. **114-117**: p. 51-62.

33. Chellam, S. and M.R. Wiesner, *Fluid mechanics and fractal aggregates.* Water Research, 1993. **27**(9): p. 1493-1496.

34. Tang, P. and J.A. Raper, *Modelling the settling behaviour of fractal aggregates–a review.* Powder Technology, 2002. **123**(2): p. 114-125.

35. Adachi, Y., *Sedimentation and electrophoresis of a porous floc and a colloidal particle coated with polyelectrolytes.* Current Opinion in Colloid & Interface Science, 2016. **24**: p. 72-78.

36. Khelifa, A. and P. Hill, *Models for effective density and settling velocity of flocs*. Vol. 44. 2006. 390-401.

37. Huang, H., *Fractal properties of flocs formed by fluid shear and differential settling.* Physics of Fluids, 1994. **6**(10): p. 3229-3234.

38. Johnson, C.P., X. Li, and B.E. Logan, *Settling velocities of fractal aggregates.* Environmental Science & Technology, 1996. **30**(6): p. 1911-1918.

39. Kestin, J., M. Sokolov, and W.A. Wakeham, *Viscosity of liquid water in the range −8 °C to 150 °C.* Journal of Physical and Chemical Reference Data, 1978. **7**(3): p. 941-948.

40. Jones, G. and S.K. Talley, *The viscosity of aqueous solutions as a function of the concentration.* Journal of the American Chemical Society, 1933. **55**(2): p. 624-642.

41. Akbari, S., S.M. Mahmood, I.M. Tan, H. Ghaedi, and O.L. Ling, *Assessment of polyacrylamide based co-polymers enhanced by functional group modifications with regards to salinity and hardness.* Polymers, 2017. **9**(12): p. 647.

42. Kim, S. and A.M. Palomino, *Polyacrylamide-treated kaolin: A fabric study.* Applied Clay Science, 2009. **45**(4): p. 270-279.

43. G. Mezger, T., *The rheology handbook: For users of rotational and oscillatory rheometers*. Vol. Hanover, Germany. 2002. 299.

APPENDIX A

This section provides assurance for the quality control measures taken for measurements of size and settling velocity as described in 2.4. Figure 19 left panel shows the raw settling velocity of flocs monitored. The images show significant changes in floc settling speeds potentially due to wall effects, particles not maintaining their constant (terminal) velocity, or interacting with other particles. The Python code developed eliminated such spurious data, identifying only the constant settling velocity of individual flocs. Figure 19 right panel shows the settling velocity data after performing such QA/QC measures on the left panel. A minimum of 500 such tracks were employed for data analysis.

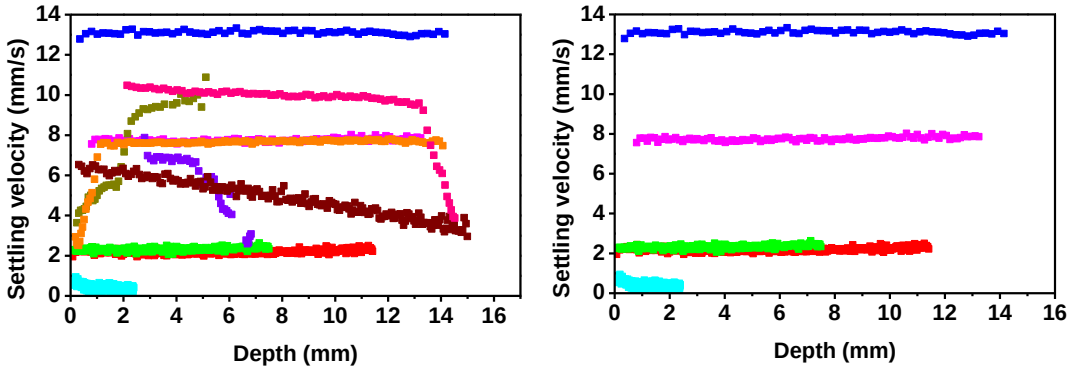

Figure 19. Quality assurance of settling velocity data.

APPENDIX B

Figure 20 shows temperature profiles monitored during jar testing and settling column experiments. As observed, the temperature remained constant throughout the duration of each experiment, i.e. isothermal conditions were maintained allowing comparisons between each laboratory test.

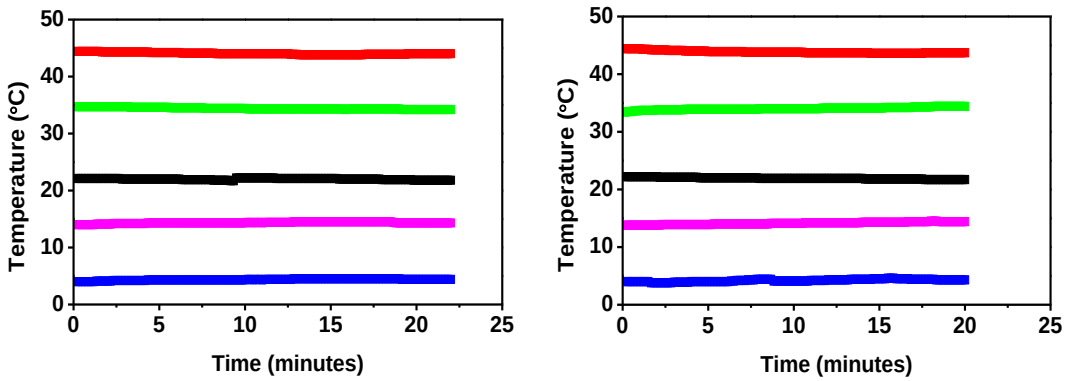

Figure 20. Temperature control during jar test (left panel) and settling column (right panel) experiments.

APPENDIX C

Measurements of Thermo Scientific^{TM} E7 test liquid standard (5 mPa.s) and deionized water were used as quality control. As shown in Figure 21, the viscosity of ultrapure water at 20 °C was measured as 1.04 mPa.s representing only a 4% deviation from the standard value of 1 mPa.s demonstrating strong quality control [39]. The E7 standard was also measured within 4%. The high salt concentration in produced water increased its viscosity by 40% compared to ultrapure water (1.40 mPa.s) presumably due to the electrostatic arrangement of ions restricting the flow of water molecules [40]. As expected, both the ultrapure and produced water behaved in a Newtonian fashion over the 3.5-decades of shear rates investigated.

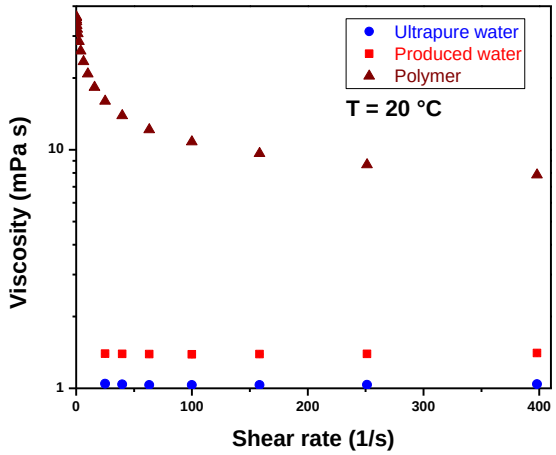

Figure 21. Viscosity of ultrapure water, produced water and polymer at 20 °C.

Also as expected, the polymer viscosity was considerably higher than the water samples (e.g. 16 mPa.s at 25 1/s). It exhibited shear thinning rheology [41, 42] attributed to disentanglement of polymer chains causing its viscosity to decrease at higher shear rates [41, 43].

APPENDIX D

Experiments at a polymer dose of 0.1% v/v and two different temperatures (22 and 44 °C) were repeated to assess their reproducibility. The average floc size and settling velocity of these experiments are summarized below in Table 4 and graphically in Figure 22. Qualitatively similar average floc sizes and settling velocities are shown in Figure 22 whereas Table 4 quantitatively analyzes experimental precision. The relative percent difference (RPD) and coefficient of variation (CV) in all cases were < ~10% demonstrating the high precision of these data and implementation of strong quality control and quality assurance protocols. In other words, jar tests were statistically reproducible allowing the comparison of floc size and settling velocity data from experiments performed at different temperatures.

Table 4. Statistical evaluation of experimental precision using average floc sizes and sedimentation rates from duplicate jar tests.

	Temperature: 22 °C				**Temperature: 44 °C**			
	Expt. 1	Expt. 2	RPD (%)	CV (%)	Expt. 1	Expt. 2	RPD (%)	CV (%)
Average size (mm)	0.89	0.85	4.71	3.25	0.35	0.39	10.8	7.64
Average settling velocity (mm/s)	4.56	4.19	8.46	5.98	3.08	3.28	6.29	4.45

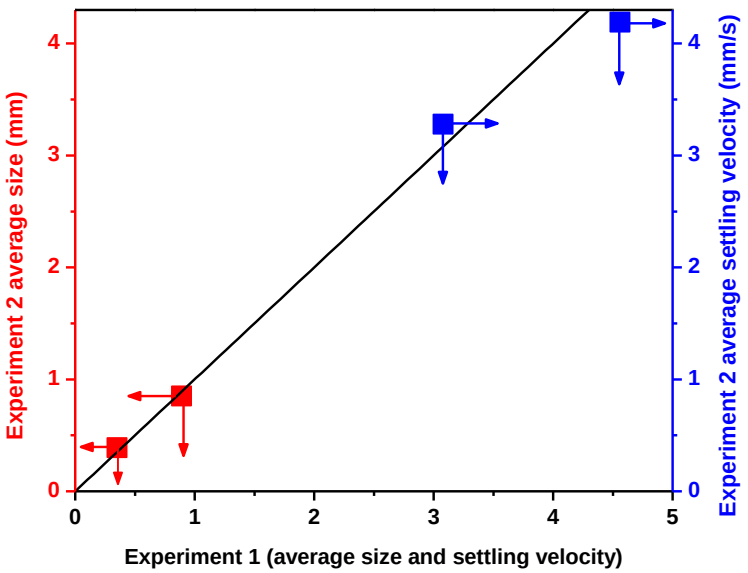

Figure 22. Reproducibility of jar tests demonstrating qualitatively similar average floc size (left y-axis) and average settling velocity (right y-axis).